Supporting information for

Potential-induced high-conductance transport pathways through single-molecule junctions

Parisa Yasini*[1], Sepideh Afsari*[1], Haowei Peng*[2], Piret Pikma[1], John P. Perdew[1, 2], Eric Borguet[1†]

[1]Department of Chemistry, Temple University, Philadelphia, PA 19122, USA

[2]Department of Physics, Temple University, Philadelphia, PA 19122, USA

Contents:

† Corresponding author: eborguet@temple.edu
*These three authors contributed equally to this manuscript

1. Chemicals and solutions:

0.05 M sulfuric acid (H_2SO_4) made from ultrapure H_2SO_4 (99.999%, Sigma-Aldrich).
0.1 mM Tetafluorotherephthalic acid (TFTPA) solution made from TFTPA, Sigma-Aldrich in 0.05 M sulfuric acid.
A single crystal Au(111) disk electrode (10 mm diameter, 2.0 mm thick, MaTeck, Germany)
Tungsten wire (0.25 mm diameter, Premion, 99.95%, Alfa Aesar)
Platinum wire (0.20 mm diameter, Alfa Aesar)
Gold wire (0.25 mm diameter, Premion, 99.998%, Alfa Aesar)
DI Water from Thermoscientific Barnstead Easypure II purification system equipped with a UV lamp (resistivity: 18.2 MΩ.cm)

2. STM cell setup and sample preparation:

A single crystal substrate electrode (disc: 10 mm diameter, 2.0 mm height) oriented to expose the Au(111) surface was used as a working electrode for imaging and conductance measurement experiments. STM tips were prepared by electrochemically etching 0.25 mm tungsten wire in 2M NaOH solution using a platinum ring electrode.[1] Tips for SMC measurements were prepared by electrochemically etching gold wire (0.20 mm diameter, Premion, 99.998%, Alfa Aesar) in a C_2H_5OH: HCl (1:1) solution.[2] Platinum wires were used as the reference and counter electrodes in electrochemical STM measurements. All the tips were coated with melted polyethylene to limit the faradic current to less than 10 pA at 100 mV bias in an electrochemical environment.[3]

Prior to all experiments, all the glassware, single crystal substrates, Teflon holder, O-ring and electrodes were first cleaned with piranha solution (H_2O_2 (30%):H_2SO_4 (concentrated, 96%) = 1:3) and rinsed more than 10 times with ultraclean deionized water from Thermoscientific Barnstead Easypure II purification system. To avoid contamination while transferring these pieces for cell setup, the gold crystal, the O-ring and the Teflon holder were covered and heated in DI water. Then the gold substrate was annealed in a hydrogen flame for 2 minutes followed by immediately quenching in hydrogen-saturated ultraclean water. Then the gold crystal, the O-ring and the Teflon holder were quickly assembled into the electrochemical STM cell. The gold electrode was covered with electrolyte immediately to avoid contamination. Then the platinum

reference and counter electrodes were inserted into the cell and immersed in the electrolyte solution. Under potential control, two/three drops of 0.1 mM TFTPA solution were added to the STM cell containing the electrolyte.

3. Electrochemical scanning tunneling microscopy (EC-STM) imaging:

All the STM images recorded with a PicoScan STM system (Molecular Imaging) under constant current mode at room temperature in the electrochemical environment. The PicoStat bipotentiostat (Molecular Imaging) used to control the tip and substrate potential, independently. 1 nA/V gain current preamplifier used for all imaging. Tungsten STM tips were prepared by electrochemically etching 0.25 mm diameter tungsten wires in 2 M NaOH solution using a platinum ring electrode. Then rinsed with acetone and DI water and coated with melted polyethylene to avoid faradic current at 100 mv bias in an electrochemical environment. Length and width of single TFTPA molecule obtained from the cross section analysis of STM image of TFTPA on negatively charged gold as 0.9 nm and 0.3 nm, respectively. These numbers are consistent with the length of TFTPA measured with ChemDraw software and indicate that the TFTPA molecules are oriented with benzene ring parallel to the Au (111) surface.

4. Electrochemical scanning tunneling microscopy-break junction (EC-STM-BJ) measurement

Single molecule conductance measurements were performed using the scanning tunneling microscopy-break junction (STM-BJ) method with a PicoScan STM system (Molecular Imaging) in an electrochemical environment. A 1000 nA/V gain current preamplifier used for all SMC measurements. In this method using STM software, the electrochemically etched gold sharp STM tip is brought into contact with the gold substrate through switching off the feedback loop. It is crashed into the gold surface and reached the maximum current that preamplifier can measure, and then withdrawn from the surface. As it withdraws, it can form a nano contact Au-Au junction with a quantum of conductance ($G_0 = 2e^2h = 7.75 \times 10^{-5}\ S$). The tip was then retracted (Tip retraction rate: 0.016 μm.s^{-1} - 0.025 μm.s^{-1}) to break the contact and a nano gap can be formed between tip and gold surface (Figure S1). In presence of molecules on the gold substrate, a single molecule can be wired in the nano gap and the electrical conductance of the molecule can be measured. The current versus distance traces were recorded during the retracting process. The process of the forming and breaking of junctions was repeated many times and a large number of current-distance traces were recorded, typically 2000-4000 traces per applied bias in our experiments for statistical analysis.

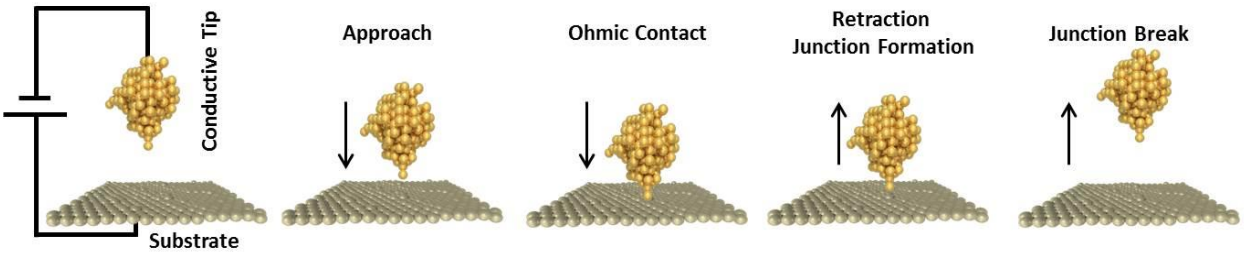

Figure S1. Principle of the scanning tunneling microscopy break-junction (STM-BJ) process.

5. Detailed analysis of STM images of TFTPA

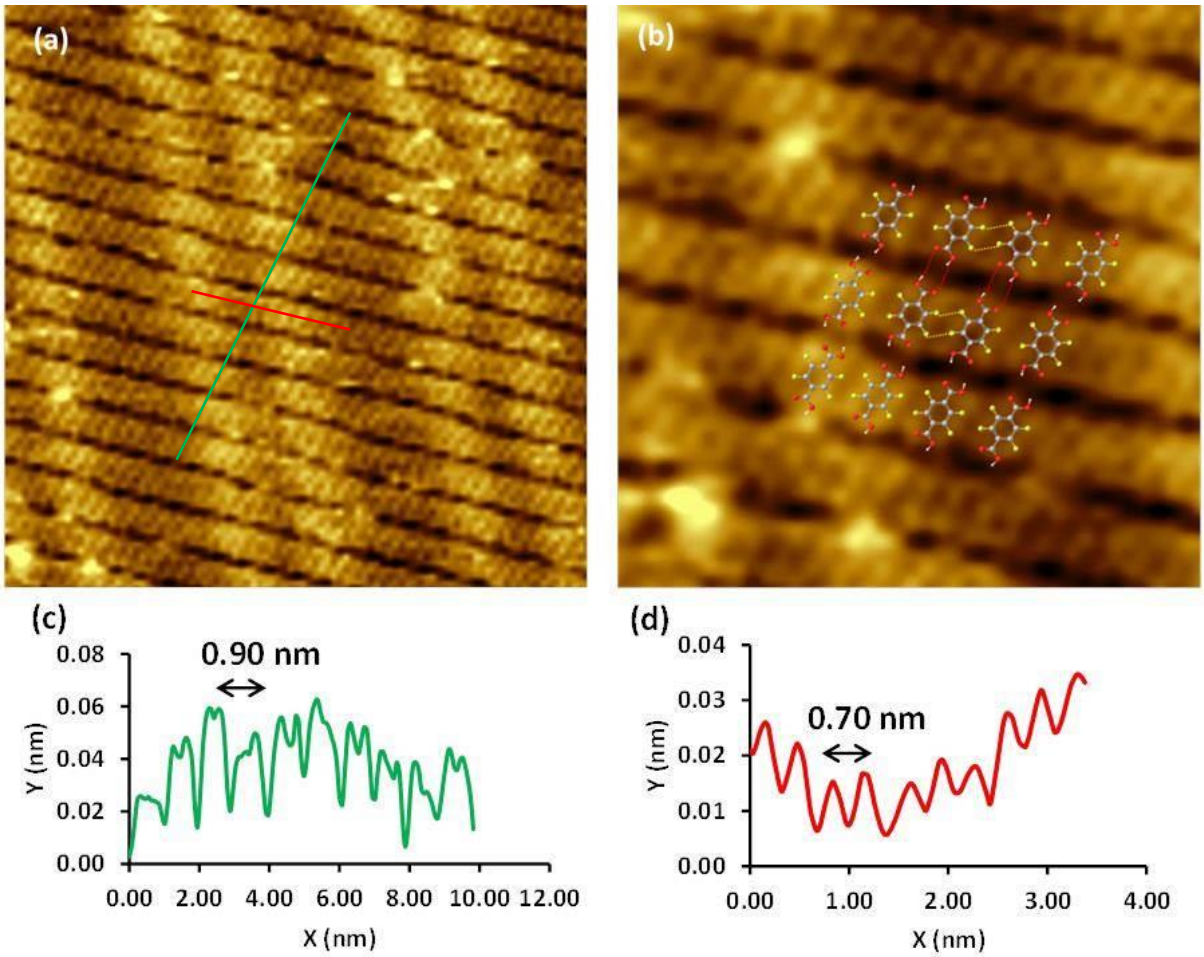

Figure S2. STM images and cross section analysis of TFTPA on a negatively charged (V_S = 0 V_{SCE}, I_t= 0.1 nA) Au (111). (a) 15×15 nm^2 STM images of TPA. (b) The proposed molecular structure of TPA, 6×6 nm^2, red and yellow dashed lines represent hydrogen bonding and halogen-halogen interaction, respectively. (c) Cross section of the ordered structure in the direction specified by the green line. (d) Cross section of the ordered structure in the direction specified by the red line.

6. Rejected current-distance curves

During our data selection procedure, the following curves were excluded from the selected curves to create current histogram.

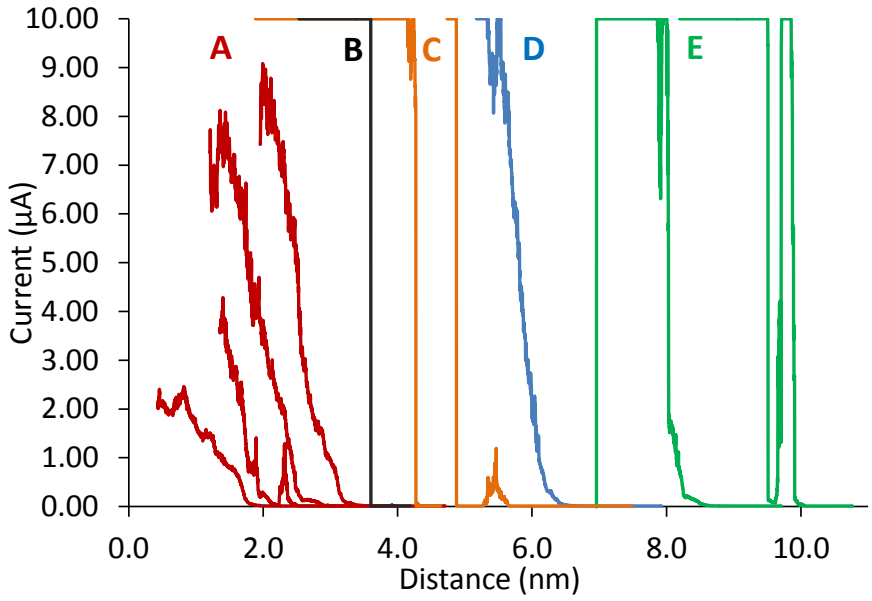

Figure S3. STM-BJ sample of individual current distance rejected curves collected in 0.05 M H_2SO_4 at V_S= 0 V_{SCE} and V_{bias}= 0.10 V_{SCE}

A) Curves that do not reach the saturation point, i.e., the maximum current that preamplifier can measure, at closest approach to the surface are excluded using the procedure written in the Igor Pro software

B) Curves where no step is observed are excluded one by one by manual inspection.

C) Curve with noise (current fluctuations above 9 μA and below 0.5 μA) while the tip is contacting surface or breaking junction, are excluded one by one by manual inspection.

D) Curves that do not drop sharply are excluded one by one by manual inspection.

E) Noisy, non-monotonic curves are excluded using file size separation. These types of curves have a larger size (296 kB) relative to normal curves size (148 kB).

7. Single molecule conductance vs sample bias:

To substantiate that the observed SMC peak is a signature of single TFTPA molecules, SMC experiments were carried out with different biases and the data histograms generated using the procedure described in the paper (Figure S4). As shown in Figure S4, the current maximum associated with the TFTPA conductance increases linearly with bias, indicating the bias independent molecular conductance indicating the Ohmic behavior of TFTPA molecule.

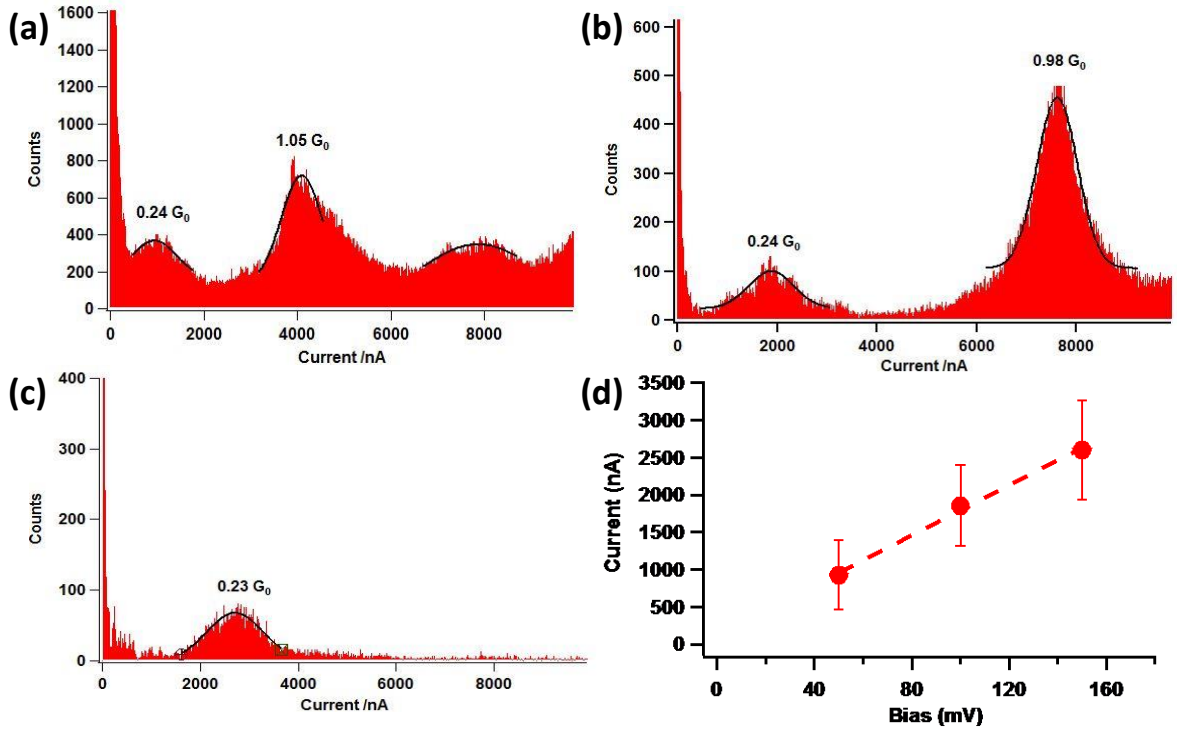

Figure S4. Histogram analysis of STM-BJ experiments of TFTPA carried out at different biases, V_S = 0 V_{SCE}: (a) All data 2251 curves at V_{bias}= 0.05 V (b) Data selection of 615 curves out of 3075 curves at V_{bias}= 0.10 V (c) Data selection of 427 curves out of 1539 curves at V_{bias}= 0.15 V (d) linear fitting of TFTPA current *vs* sample bias. Error bars are the full half width maximum (FHWM) of each peak as it appeared in the conductance histograms constructed at different biases.

8. Single molecule conductance vs sample potential

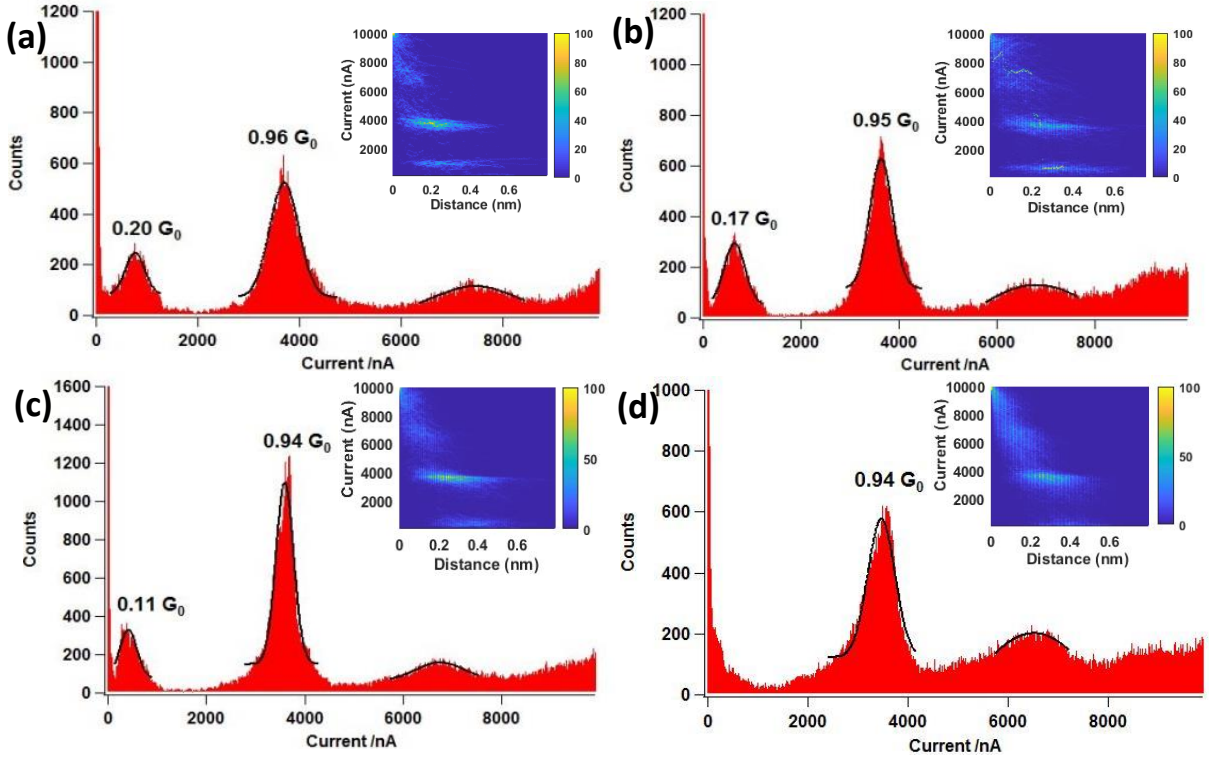

Figure S5. Histogram analysis of the STM-BJ experiments on TFTPA carried out at V_{bias}= 0.05 V at different sample potentials: (a) Data selection of 394 curves out of 1519 curves at V_S= 0.1V_{SCE} (b) Data selection of 510 curves out of 2241 curves at V_S= 0.20 V_{SCE} (c) Data selection of 561 curves out of 2268 curves at V_S= 0.35 V_{SCE} (d) 829 curves out of 2548 at V_S= 0.65 V_{SCE} (e) linear fitting of TFTPA current *vs* sample potential. Insets are 2D current histograms constructed from the same number of curves used for 1D histograms.

9. Detailed analysis of STM images of TPA

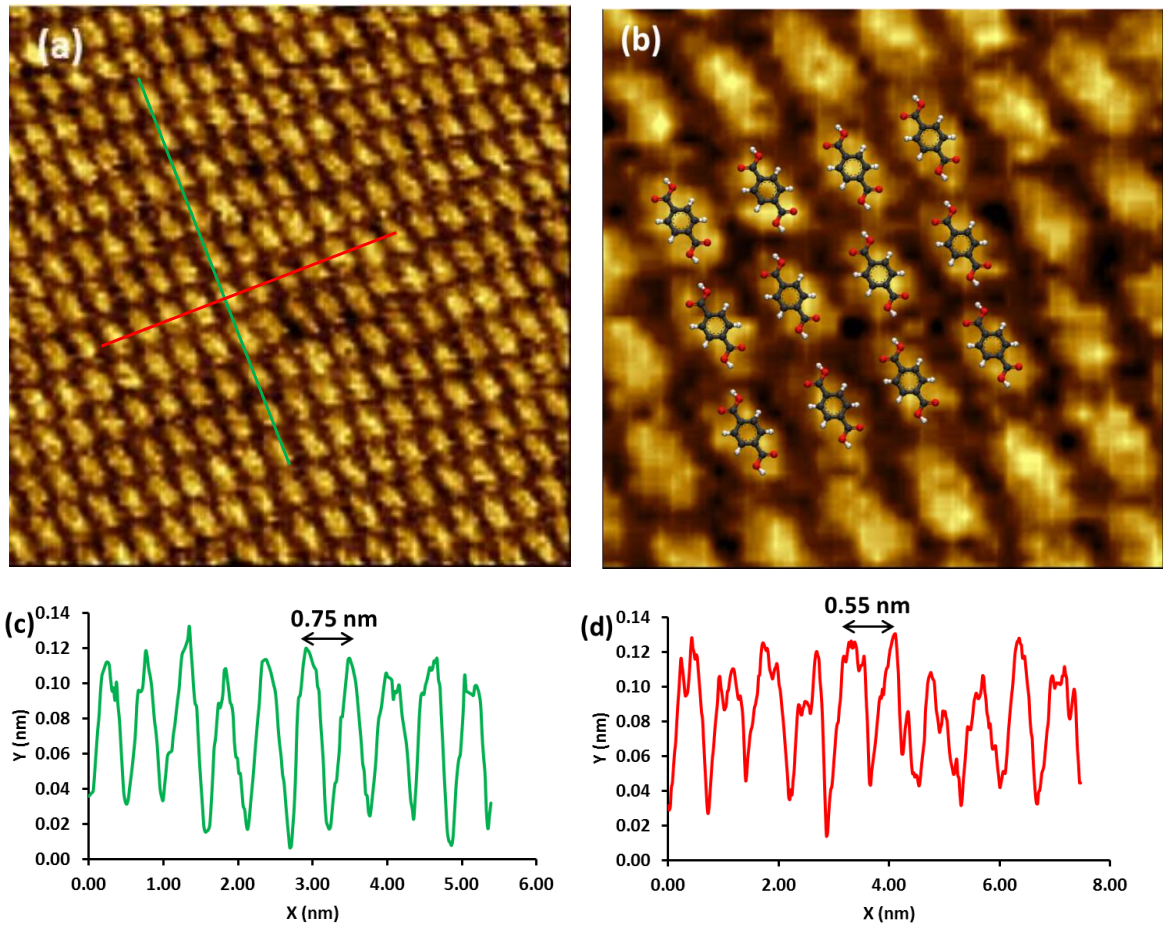

Figure S6: STM images and cross section analysis of TPA on a negatively charged (V_S = 0 V_{SCE} , I_t= 0.1 nA) Au (111). (a) 10×10 nm^2 STM images of TPA. (b) The proposed molecular structure of TPA, 3.5×3.5 nm^2 (c) Cross section of the ordered structure in the direction specified by the green line. (d) Cross section of the ordered structure in the direction specified by the red line.

10. One and two-dimensional histograms of TPA

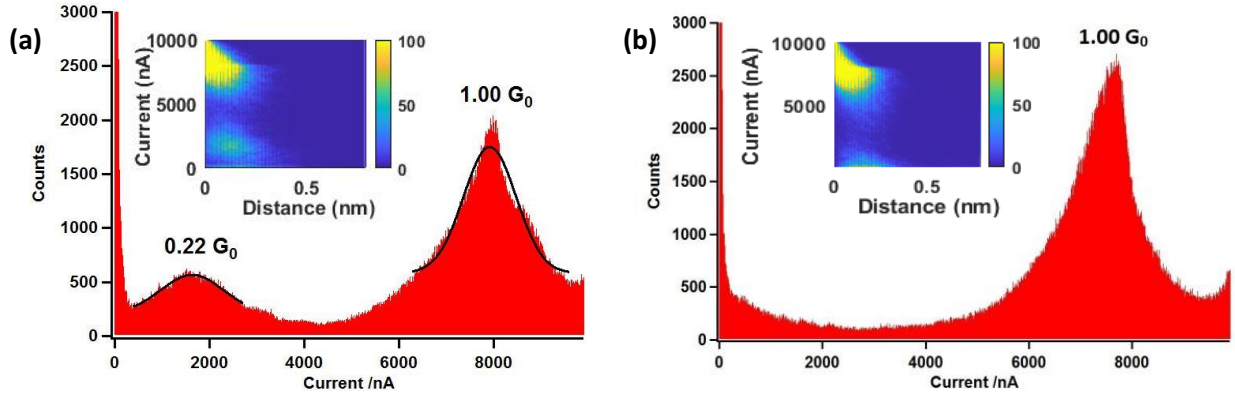

Figure S7. Current histograms of TPA in 0.05M H_2SO_4 on (a) negatively charged Au(111), V_S = 0 V_{SCE} and (b) V_S= 0.70 VSCE. Insets are 2D histograms constructed from the same plotted using same number of curves used for the 1D current histograms.

11. Single molecule conductance control experiments

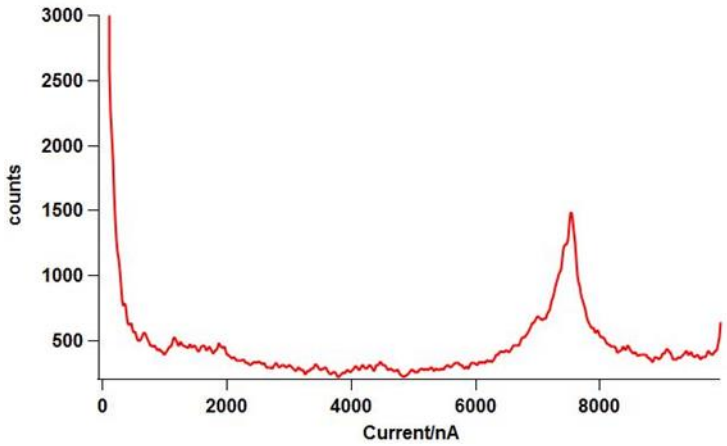

Figure S8. Single molecule conductance control experiments on Au (111). Current histograms of 0.05M H_2SO_4 without TFTPA on negatively charged Au(111) (V_S = 0 V_{SCE} and V_{bias} = 0.10 V).

No well-defined peak except for an Au-Au junction was observed in the control experiments in 0.05M H_2SO_4 without TFTPA molecules on negatively charged Au (111) in a range of 0-10000 nA.

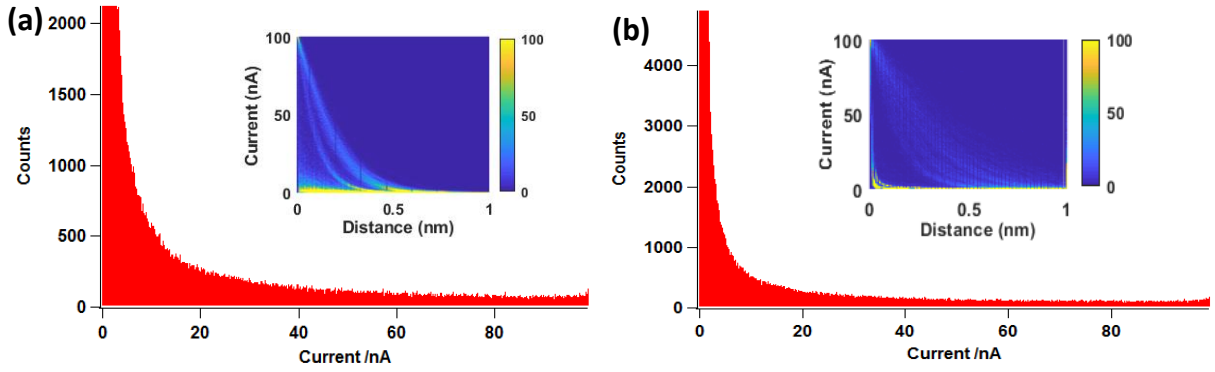

Figure S9. Control experiments of single molecule conductance of TFTPA on Au (111) at lower current. (a) All curves (2123)1D current histogram measured in 0.05 M H_2SO_4 with 0.1 mM TFTPA at V_S= 0 V_{SCE}, V_{bias}=0.1 V, inset: 2D current histogram. (b) All curves (3971) 1D current histogram measured in 0.05 M H_2SO_4 with 0.1 mM TFTPA at V_S= 0.65 V_{SCE}, V_{bias}=0.1 V, inset: 2D current histogram.

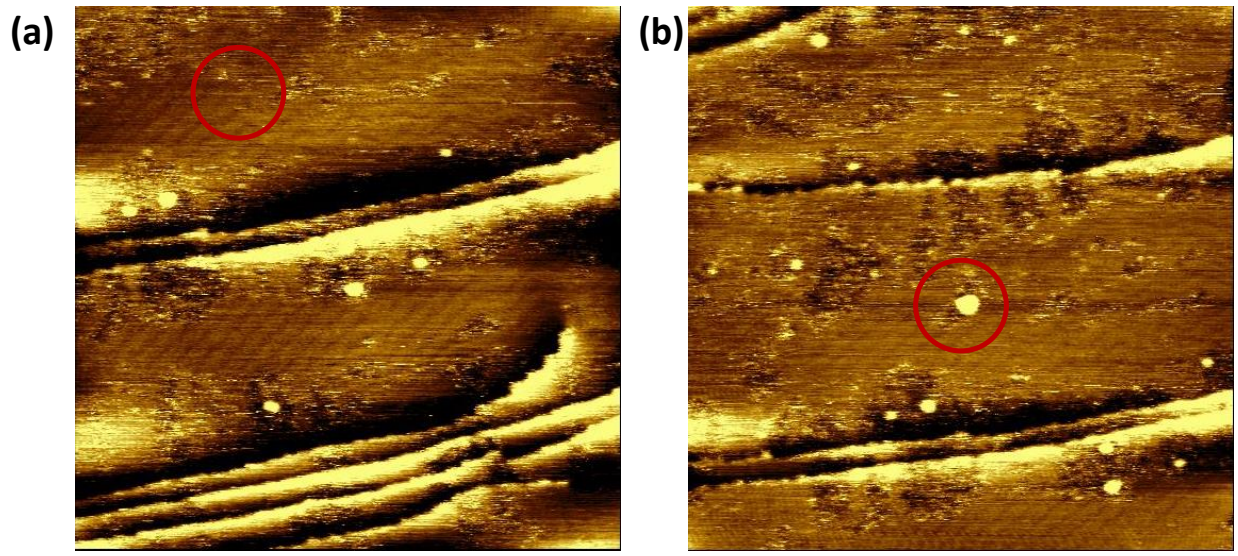

Figure S10. STM image of ordered hexadecane before and after STM-BJ on Au(111), I_t= 1 nA, V_{bias}= 0.1 V, scan area:2×2 μm^2: (a) Before break junction measurement. (b) After break junction measurement. The same Au tip was used for imaging and break junction measurements.

To test the stability of the ordered structure and the tip perturbations after the break junction process, STM images of ordered hexadecane on Au(111) were recorded (Figure S10 (a)). The surface was imaged immediately after performing the break junction procedure and measuring ten current-distance curves with the same gold tip (figure S10(b)). The STM image shows that the spots where the tip landed are locally disturbed (red circle) but the ordered molecular structure remained unaffected around the junction formation areas. In addition, the observed drift in a normal lab environment (ambient temperature and pressure) after measuring ten current-distance curves is ~ 60 nm per scan of 2×2 μm^2 area. This relatively large lateral drift is associated with the tip movement in Z direction during the approach and retracts process. Therefore, the average tip drift per approach and retract curve is on the order of 6 nm, indicating that the tip will not land on the same spot for each junction that is formed. Furthermore, the fact that we can record high-resolution images after the break junction strongly indicates that the tip does not undergo a destructive crashing and deformation during the break-junction measurement process.

12. Computational details:

The first-principles calculations and the non-equilibrium Green's function (NEGF) transport calculations are performed with the SIESTA package[4] and the TranSIESTA code[5] therein. The Troullier-Martins norm-conservation pseudopotentials[6] are used, and the so-called SZP pseudo-atomic orbital (PAO) basis for Au, and DZP for other elements are employed. The consistent exchange van der Waals density functional (vdW-DF-cx)[7] is used to take into account the weak interaction between the surface and molecules. The convergence with respect to the mesh cutoff and the k-meshes for both the relaxation and NEGF calculations have been carefully checked.

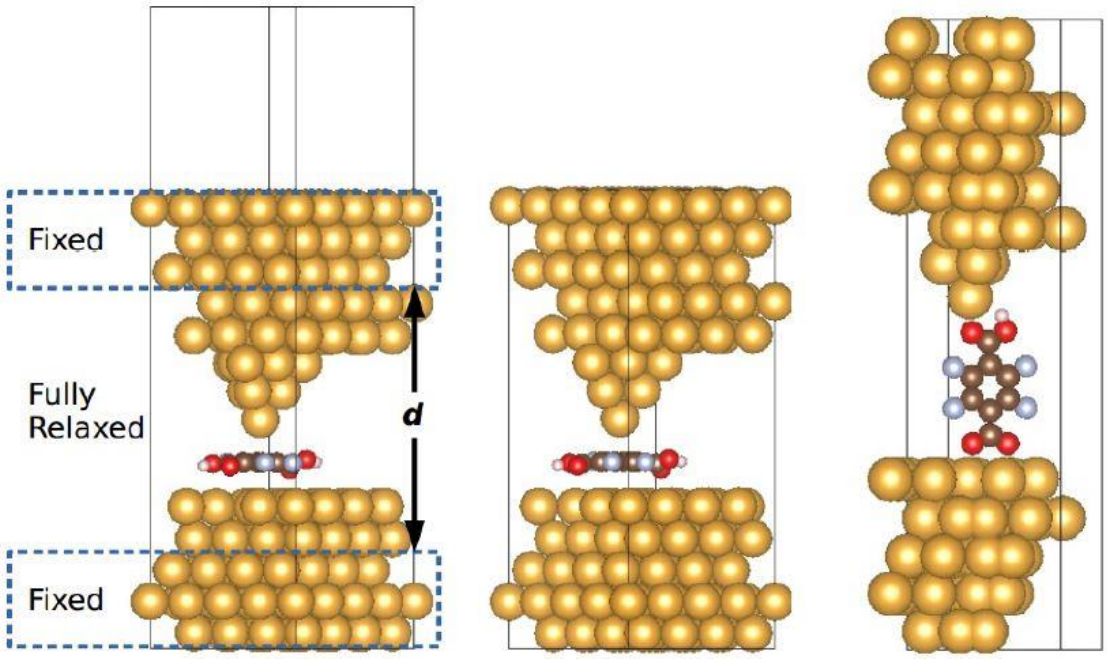

Figure S11. Schematic illustration for the structure modeling in this work. Left: the supercell for the flat configuration with which we vary the electrode-substrate distance *d* manually and relax the atoms between the two bottom and top triple-layers; Middle: the final lowest-energy (as function of *d*) supercell with the vacuum layer removed for following NEGF calculation, where semi-infinite electrodes will be attached to both ends; Right: similar to Middle but for the vertical configuration.

For the flat configuration, a 5-layer 4 ×4 × 1 supercell is used to model the Au(111) surface, and a 5-layer 3 × 3 × 1 supercell for the vertical molecular configuration. We first determined the structure of the molecular junction as shown in the left panel for Figure S8, which, from the

bottom to the top, contains the 5-layer Au(111) surface electrode, the molecule with the so-called hcp configuration, the Au(111) tip, another 5-layer Au(111) surface, and a vacuum layer about 15 Å. We change the distance between the top and bottom Au triple-layers by a step of 0.1 Å, and let the other atoms fully relax until the residual forces are smaller than 0.04 eV/ Å. Such obtained optimal distance between the gold surface and tip is about 5.55 and 5.34 Å in the cases of TFTPA and TPA single molecular junctions, respectively. Then the resulting lowest energy structures with the vacuum layer removed are used for the following NEGF calculations (Middle panel in Figure S8 for the flat configuration). A similar procedure was applied to obtain the structure for the vertical configuration (Figure S8 Right panel), where the bottom hydrogen atom was removed and the Au-O bond forms as the anchoring group. The gate voltage is applied by raising or lowering the electrostatic potential in the box around the molecule (the distance between the top and bottom boundaries to the Au atoms is about 0.5 Å) according to the method implemented in Ref. 5.

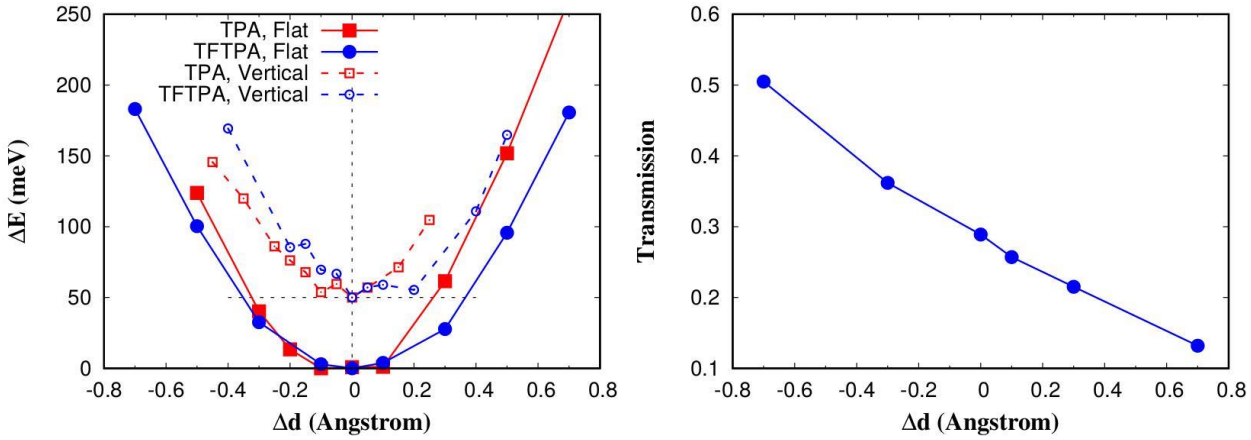

Figure S12. Left: The calculated energy-distance relationship for the four single molecule junctions. Both the energies and distances (***d*** as defined in Figure S11) are referenced to those at the lowest-energy ***d***, and the curves for the vertical configurations have been raised up by 50 meV for clarity. Right: the calculated zero-bias transmission at the Fermi level at selected distances for TFTPA. We expect a similar dependence for the TPA molecule junction with the flat configuration, and the changes in conductance for the vertical configuration should be much smaller.

In Figure S12 Left, we show the (relative) total energies with respect to the lowest-energy structure for all the four single molecule junctions. For both TPA and TFTPA with the flat configuration, the curves are quite smooth, nearly symmetric and quite flat around the optimal distance. While for the vertical configuration, the curves are less smooth which may due to the complex structure relaxations. For the vertical configuration, since the molecule is directly bonded with both electrodes, the molecule remains at the middle as the distance changes. While for the flat configurations, we do find that the change of the separation between the benzene ring and the tip is about 1.5 times as large as that between the benzene ring and the Au(111) surface as ***d*** changes. In general, within the range of distance changes considered, the molecules do not tend to adhere to either the tip or surface. In the Right panel, we show the calculated low-bias conductance (approximated by the zero-bias transmission at the Fermi level), for the TFTPA single molecule junction with the flat configuration, as the distance ***d*** changes. A nearly linear trend presents, but no drastic (orders of magnitude) change of the conductance occurs even when the distance ***d*** is increased or decreased by 0.7 Å.

The observed difference between the apparent independence of the experimental conductance as the junction is extended and the calculated transmission spectra versus distance might stem from the specific details of the molecular junction in the experiment which have not been considered in the calculation such as:

(1) The tip atoms may rearrange as the junction elongates and, therefore, the distance between Au atoms on either side of the junction remains roughly constant as the tip retracts. In the experiment the limitless number of Au atoms in the electrodes will dissipate any strain, and the metal-molecule-metal junction will be less affected by the stretching of the junction and the junction stays closer to the lowest energy configuration (energy minimum in Figure S12). Hence, the conductance doesn't change as much over 2 Å of elongation. However, by necessity, the calculations are done with a finite/limited number of Au atoms, which does not allow for the same strain dissipation as in the experiment.

(2) The tip in experiments may move around laterally (the lateral drift in each formation and breaking of a junction is calculated to be on the order of ~ 6 nm), and will land on different parts of the molecule. For simplicity, in the calculation it is always located on the top of the benzene ring center.

(3) An ideally flat surface and flat configuration are considered here, which may also differ from the experimental structures as discussed in the manuscript.

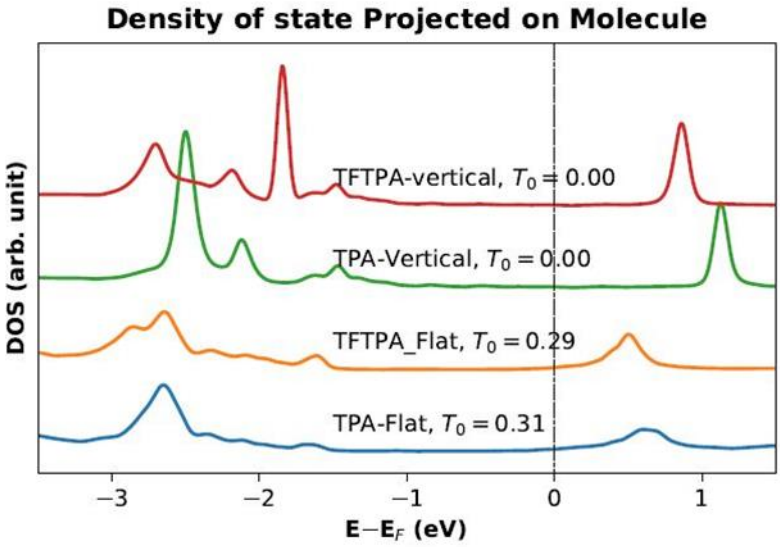

Figure S13. The projected density of states of the molecules in the single molecule junction. The zero energy is set at the Fermi level.

In Figure S13, we provide the density of states projected on the molecules at the zero-gate voltage (with a wider energy window compared to Figure 6 in the main text). The LUMO-like state shows as the main peak about 0.5-0.6 eV above the Fermi level energy, while the HOMO-like state first occurs near about 1.5-1.6 eV below the Fermi level in energy.

References:

(1) Ju, B.-F.; Chen, Y.-L.; Ge, Y. The art of electrochemical etching for preparing tungsten probes with controllable tip profile and characteristic parameters. *Rev. Sci. Instrum.* **2011**, *82*, 013707.
(2) Baghernejad, M.; Manrique, D. Z.; Li, C.; Pope, T.; Zhumaev, U.; Pobelov, I.; Moreno-Garcia, P.; Kaliginedi, V.; Huang, C.; Hong, W.; Lambert, C.; Wandlowski, T. Highly-Effective Gating of Single-Molecule Junctions: An Electrochemical Approach. *Chem. Commun.* **2014**, *50*, 15975-15978.
(3) Tuchband, M.; He, J.; Huang, S.; Lindsay, S. Insulated gold scanning tunneling microscopy probes for recognition tunneling in an aqueous environment. *The Review of Scientific Instruments* **2012**, *83*, 015102.
(4) Soler, J.; Artacho, E.; Gale, J.; Garcia, A.; Junquera, J.; Ordejon, P.; Sanchez-Portal, D. The SIESTA method for ab initio order-N materials simulation. *Journal of Physics-Condensed Matter* **2002**, *14*, 2745-2779.

(5) Papior, N.; Lorente, N.; Frederiksen, T.; Garcia, A.; Brandbyge, M. Improvements on non-equilibrium and transport Green function techniques: The next-generation TRANSIESTA. *Comput. Phys. Commun.* **2017**, *212*, 8-24.
(6) Troullier, N.; Martins, J. Efficient Pseudopotentials for Plane-Wave Calculations .2. Operators for Fast Iterative Diagonalization. *Physical Review B* **1991**, *43*, 8861-8869.
(7) Berland, K.; Hyldgaard, P. Exchange functional that tests the robustness of the plasmon description of the van der Waals density functional. *Physical Review B* **2014**, *89*, *035412*.